HHS Public Access

Author manuscript

Cancer Res. Author manuscript; available in PMC 2018 March 15.

Published in final edited form as:

Cancer Res. 2017 March 15; 77(6): 1465–1475. doi:10.1158/0008-5472.CAN-16-1646.

Fibrinolytic enzyme co-therapy improves tumor perfusion and therapeutic efficacy of anticancer nanomedicine

Ameya R. Kirtane[1], **Tanmoy Sadhukha**[1], **Hyunjoon Kim**[1], **Vidhi Khanna**[1], **Brenda Koniar**[2], and **Jayanth Panyam**[1,3,*]

[1]Department of Pharmaceutics, University of Minnesota

[2]Research Animal Resources, University of Minnesota

[3]Masonic Cancer Center, University of Minnesota

Abstract

Elevated interstitial fluid pressure and solid stress within tumors contribute to poor intratumoral distribution of nanomedicine. In this study, we hypothesized that the presence of fibrin in tumor extracellular matrix contributes to hindered intratumoral distribution of nanocarriers and that this can be overcome through the use of a fibrinolytic enzyme such as tissue plasminogen activator (tPA). Analysis of fibrin expression in human tumor biopsies showed significant fibrin staining in nearly all tumor types evaluated. However, staining was heterogeneous across and within tumor types. We determined the effect of fibrin on the diffusion, intratumoral distribution, and therapeutic efficacy of nanocarriers. Diffusivity of nanocarriers in fibrin matrices was limited and could be improved significantly by co-incubation with tPA. In vivo, co-administration of tPA improved the anticancer efficacy of nanoparticle-encapsulated paclitaxel in subcutaneous syngeneic mouse melanoma and orthotopic xenograft lung cancer models. Furthermore, treatment with tPA led to decompression of blood vessels and improved tumor perfusion. Co-treatment with tPA resulted in greater intratumoral penetration of a model nanocarrier (Doxil[7reg;]), leading to enhanced availability of the drug in the tumor core. Fibrinolytics such as tPA are already approved for other indications. Fibrinolytic co-therapy is therefore a rapidly translatable strategy for improving therapeutic effectiveness of anticancer nanomedicine.

Keywords

fibrinolytics; nanoparticles; tumor penetration; fibrin; tumor perfusion

Introduction

Poor intratumoral distribution of the drug carrier and inadequate drug delivery to tumors are significant challenges to successful translation of anticancer nanomedicine (1). Prolonging circulation times (2, 3) as well as optimizing particle size, shape, charge and other

Author for correspondence: Jayanth Panyam, Ph.D., Department of Pharmaceutics, College of Pharmacy, University of Minnesota, 308 Harvard Street SE, Minneapolis, MN 55455. Phone: 612-624-0951. Fax: 612-626-2125. jpanyam@umn.edu.

Conflict of interest: J.P., T.S. and A.R.K. have a US patent application regarding the use of fibrinolytics to improve chemotherapeutic efficacy of nanoparticles

physicochemical properties of the drug carrier may address these challenges (4), but only to a limited extent. The benefits of these approaches are limited by the erratic blood supply often observed in tumors.

Tumor perfusion is limited due to several peculiar characteristics of tumor blood vessels. These include inadequate coverage of the tumor, lack of transvascular pressure gradients, and their collapsed nature (5). Blood vessels in the core of the tumor are compressed under solid stress exerted by fast-dividing cells (6) and large amounts of extracellular matrix (ECM) (7). Treatment with enzymes that degrade ECM components such as collagen (8) and hyaluronic acid (9) has been shown to improve vascular characteristics and enhance blood supply in specific tumor types. However, the ubiquitous expression of collagen and hyaluronic acid in the body may limit the widespread use of these enzymes.

Due to the leaky nature of tumor blood vessels, fibrinogen, a soluble vascular protein, is deposited in the tumor matrix. The prothrombogenic activity of tumor cells leads to the conversion of fibrinogen to cross-linked fibrin, the principle ingredient of blood clot (10, 11). In fact, due to the constitutive activity of coagulation factors in tumors, they are often considered ‘overhealing wounds’ (12). Presence of significant amounts of fibrin in the tumor matrix may contribute to increased solid stress often observed in tumors. Additionally, the tumor specific presence of fibrin makes it an attractive target for therapeutic interventions. However, the role of fibrin in limiting the intratumoral transport of drug carriers and the effect of fibrin degradation on their anticancer efficacy has not been previously studied.

We show here that administration of a fibrinolytic enzyme improves tumor perfusion by decompressing blood vessels and enhances chemotherapeutic activity of anticancer nanomedicine in syngeneic mouse melanoma and xenograft lung cancer models.

Materials and Methods

Materials

Tissue microarrays of various human tumor biopsies were obtained from Folio Biosciences (Ohio, USA). Anti-human fibrin(ogen) antibody was purchased from Dako (California, USA). Poly(lactide-*co*-glycolide) (PLGA) was purchased from Lactel (Alabama, USA). L-lactide, bovine fibrinogen, and thrombin were obtained from Sigma Aldrich (Missouri, USA). Tissue plasminogen activator (tPA) was obtained from Abcam (Massachusetts, USA). Poly(ethylene glycol) was purchased from Laysan Bio Inc. (Alabama, USA).

Staining, microscopy and analysis of human tissue microarrays

Tissue microarrays were digested with Proteinase K and stained with a polyclonal rabbit anti-human fibrin(ogen) antibody at a dilution of 1:1000. Representative images were acquired using an Eclipse TS100 microscope (Nikon instruments, New York, USA) under 400X magnification. Fraction of the area stained was quantified using ImageJ v1.48 software.

Synthesis and characterization of paclitaxel loaded PLGA nanoparticles

A block copolymer of poly(lactide) and poly(ethylene glycol) was synthesized via ring opening polymerization reaction as described before (13). The block copolymer was characterized using ^{1}H-NMR (Varian 400 MHz) (13).

PLGA nanoparticles loaded with paclitaxel were synthesized by a single emulsion technique. Nanoparticles were surface functionalized with the block copolymer using the interfacial activity assisted surface functionalization technique developed in our lab. Nanoparticles were separated from free drug by repeated (three times) ultracentrifugation and resuspension in deionized water, and then lyophilized (13). PLGA nanoparticles loaded with a fluorescent dye (coumarin 6) were synthesized similarly (14).

To determine particle size and zeta potential, nanoparticles were dispersed in deionized water and then subjected to dynamic light scattering analysis (Delsa Nano C, Beckmann Coulter, California, USA).

To determine drug loading, nanoparticles were dispersed in methanol (~1 mg/mL) and the drug was extracted overnight. Nanoparticles were separated from extracted drug by centrifugation (14000 RPM, 15 minutes). Drug concentration in the extract was analyzed using HPLC (Beckmann Coulter, California, USA) (15).

Migration across fibrin matrix

A Transwell® assay was used to determine the rate of migration of nanoparticles across fibrin matrices. In these studies, fibrin matrix was formed *in situ* in the upper insert of a Transwell® plate (12 mm diameter, 0.4 μm pore size, polycarbonate membrane). Fibrinogen (3 mg/mL) was dissolved in 0.9% w/v saline at 37°C. Plasminogen (0.1 U/mL) and thrombin (1 U/mL) were added to the fibrinogen solution. A 750-μL aliquot of the solution was then quickly transferred to the inserts. The plate was placed in a cell culture incubator overnight to allow fibrin gel formation.

At the beginning of the experiment, the bottom well was filled with 1 mL of 0.15 mM phosphate buffered saline (pH 7.4, 1X PBS). Nanoparticles (dispersed in deionized water at a concentration of 5 mg/mL; 0.1 mL) were mixed with different amounts of tPA and added on top of the fibrin matrices. At various time points, contents of the bottom well were collected and lyophilized. The bottom well was replenished with fresh 1X PBS. The lyophilized samples were extracted overnight with methanol. Concentration of paclitaxel in the extract was determined using HPLC.

To determine the lag time for the appearance of drug in the bottom chamber, a curve given by the following equation was used to fit the data:

$$A = A_0[1 - e^{-k(t - t_{lag})H(t)}]$$

where A is the cumulative amount of drug in the bottom chamber, A_0 is the amount of drug added to the top chamber, k is the rate constant for transport across the insert and t_{lag} is the lag time. H(t) is a Heaviside step function described as:

$$H(t)=\begin{cases} 0; & t<t_{lag} \\ 1; & t \geq t_{lag} \end{cases}$$

Model fitting was performed using Matlab software (Mathworks, Massachusetts, USA).

We also calculated the apparent permeability (Papp) of drug into the bottom chamber. Apparent permeability was calculated as described by Hubatsch *et al.* (16).

$$Papp=\frac{dQ}{dt}\left(\frac{1}{AC_0}\right)$$

Where dQ/dt is the mass of paclitaxel transported per unit time after the lag time, A is the surface area of the insert, and C_0 is the initial concentration of paclitaxel in the top insert.

Cell culture

B16F10 murine melanoma cells were provided by Prof. Olin (University of Minnesota). Olin lab obtained the cells from American Type Culture Collection (ATCC) with authentication by short tandem repeat. A549 human lung adenocarcinoma cells transfected with firefly luciferase gene (A549-luc) were purchased from Caliper Life Sciences (Massachusetts, USA). Both cells were cultured in Roswell Park Memorial Institute (RPMI) 1640 medium supplemented with 10% v/v fetal bovine serum and 1% v/v penicillin and streptomycin under humidified atmosphere with 5% CO_2 at 37°C.

Cellular uptake across fibrin matrix

Cellular uptake of nanoparticles across fibrin matrices was determined using a Transwell® assay. Fibrin matrices were formed in the upper inserts of the Transwell® plate as described above. B16F10 cells were seeded in the bottom well ($1X10^6$ cells/well) and allowed to adhere overnight. On the day of the experiment, media was replaced with serum free media (1 mL/well). Coumarin 6 loaded nanoparticles (0.25 mg dispersed in 0.05 mL deionized water) were mixed with increasing amounts of tPA and added on top of the fibrin matrix. After 4 h, cells were washed with cold 1X PBS, and trypsinized. The cells were then transferred to flow tubes and centrifuged at 1000 RPM for 5 minutes. The supernatant was removed and cells were suspended in cold 1X PBS. Cellular fluorescence was analyzed using flow cytometry (BDCalibur flow cytometer).

Anti-cancer efficacy of combination therapy in orthotopic xenograft lung cancer model

All animal studies were performed in compliance with protocol approved by the Institutional Animal Care and Use Committee at the University of Minnesota. The efficacy of tPA-paclitaxel combination therapy was evaluated in a mouse xenografted model of human lung cancer. The lung tumor model was set up as described before (17), with some minor changes. A549-luc cells (~$6X10^5$ cells/mouse) were dispersed in 1X PBS and injected in 4–6 week old, female, severe compromised immunodeficient (SCID) mice via the lateral tail

vein. Tumor growth in the lungs was determined by monitoring the bioluminescence using IVIS spectrum *in vivo* imaging system.

About 4–5 weeks after cell injection, animals were treated intravenously with saline or paclitaxel (40 mg/kg) or a combination of paclitaxel and tPA (436 μg/kg). The treatments were administered thrice every 96 h. Tumor bioluminescence was monitored every 3–4 days.

Anti-cancer efficacy of combination therapy in syngeneic melanoma model

B16F10 cells ($1x10^6$ cells dispersed in 0.05 mL 1X PBS) were injected subcutaneously in 4–6 week old female C57BL/6 mice. Tumor dimensions were measured daily using a digital caliper. Tumor volume was calculated as 0.5 x length x $width^2$. Treatment was initiated when the tumor volume reached ~100 mm^3. Animals were treated intravenously with saline or tPA (436 μg/kg) or paclitaxel nanoparticles (40 mg paclitaxel/kg) or a combination of paclitaxel nanoparticles and tPA. Animals were treated with three doses administered 96 h apart.

Immunohistochemistry analysis of $CD31^+$ blood vessels

Tumors from the B16F10 efficacy study were collected and fixed in 5% formalin in PBS for 48 h. The tumors were then removed from the formalin solution, washed thrice with 1X PBS, and stored in 70% ethanol until further processing. Tumor sections were stained with a goat anti-mouse CD31 antibody (Santa Cruz Biotechnology, TX, USA).

Fifty random images of each tumor section were obtained using an optical microscope at 400X magnification. Diameters of the $CD31^+$ blood vessels were measured using ProgRes® Capture software (Jenoptik AG, Germany). On an average, each image contained 2–3 blood vessels. Six sections from each treatment group (2 sections x 3 animals/group) were analyzed. Hence, the results represent ~600–900 blood vessels/treatment group.

Ultrasound imaging of B16F10 tumors

C57BL/6 mice were shaved and inoculated with B16F10 cells as described in the efficacy study. When tumors reached a volume of ~100 mm^3, animals were randomly assigned to two groups and treated with three doses of either saline or tPA (436 μg/kg) every 96 h. About 1 h after each treatment, tumor perfusion was analyzed using ultrasound imaging.

Ultrasound imaging was performed using a Vevo® 2100 system (FujiFilm VisualSonics). Animals were anesthetized using isoflurane, and were maintained on the gas throughout the imaging. Any hair on the tumor was removed using Nair™ (Church and Dwight). Using a motorized stage, an MS550 probe was placed on top of the tumor. An appropriate field of view was determined by monitoring tumor boundary and location in B-mode. Perfusion area was visualized by switching to the Power Doppler mode. Power Doppler images were analyzed using the ImageJ v1.48 software.

Intratumoral and intra-organ distribution of Doxil

C57BL/6 mice bearing B16F10 tumors were used for these studies. Tumors were established as described before. When the tumor volume reached ~100 mm^3, animals were treated with

either saline or tPA (436 μg/kg). Four days later, animals were treated with Doxil® (20 mg doxorubicin/kg) or a combination of Doxil® and tPA. On the next day, animals were sacrificed and their tumors were collected. Tumors were embedded in Tissue-Tek® optimum cutting temperature (OCT) compound (Sakura Finetek USA, Inc., CA, USA) and flash frozen in a slurry of dry ice in isopentane. Liver, lungs, spleen and brain were harvested and processed similarly.

Tumor or tissue sections (5 μm thickness) were cut and analyzed using a Nikon A1Rsi confocal super resolution microscope (Nikon Instruments Inc., NY, USA). Fluorescence and transmitted light images were obtained at 10X magnification. For fluorescence imaging, samples were excited using a 488 nm laser, and emitted light was collected at 595/50 nm. Using a motorized stage, serial images were obtained across the entire tumor section. Images were stitched together using NIS Elements Viewer 4.0 software (Nikon Instruments Inc., NY). A region of interest (ROI) was drawn manually around the periphery of the tumor, and total fluorescence intensity and area of the ROI was measured. The ROI was shrunk to ~40% and ~10% of its original area, and similar measurements of fluorescence intensity and area were carried out. Fluorescence intensity normalized to area in the central 40% and central 10% of the tumor section relative to total fluorescence intensity was measured and used as an indicator of penetration of the drug into the core of the tumor.

Statistical analyses

Statistical analyses for matrix migration and cell uptake studies were performed using One-way ANOVA. For efficacy studies and ultrasound analysis, statistical significance of the differences between two treatment groups was determined using Student's t-test. For all studies, $p<0.05$ was considered statistically significant.

All other methods are described in Supplemental information.

Results

Extensive fibrin deposition in various tumors

Several solid tumors have leaky blood vessels. This leads to the deposition of vascular proteins in the tumor matrix. We were particularly interested in analyzing the deposition of fibrin, an important vascular protein involved in blood clotting.

We examined the occurrence of fibrin in an array of human tumor biopsies. We found that all the tumors considered in our studies showed significant fibrin deposition (Figure 1A–H). Fraction of the tumor area stained for fibrin ranged from ~20–90% (Figure 1I). We next determined if fibrin levels were affected by the stage of the disease, metastatic status, or the type of cancer. To minimize variability, we considered only lung carcinomas. We found that both, adenocarcinomas, and squamous cell carcinomas, had comparable amounts of fibrin (Figure 1J). These levels were unaffected by the stage of the disease (Figure 1K) or the presence of lymph node metastasis (Figure 1L). Representative images of lung carcinomas in different stages of progression are shown in Figure S1.

We also analyzed expression of fibrin in several human and murine tumors grown in mice. Similar to our results with the human tumor samples, high levels of fibrin were found in these tumors as well (Figure S2). These results corroborated well with previous findings that fibrin is an important component of the tumor ECM (18, 19).

tPA improves diffusivity of nanocarriers *in vitro*

Previous reports have shown that degrading other components of tumor ECM such as hyaluronic acid and collagen can improve delivery of drugs to tumor cells. This result is manifested as both enhanced intratumoral distribution of the drug as well as improved tumor perfusion (9, 20, 21). We determined whether degrading fibrin in tumors had a similar effect. To degrade fibrin within tumors, we used tPA, an enzyme that is used clinically to treat patients with pulmonary embolism, myocardial infarction and stroke (22–24).

PLGA nanoparticles loaded with paclitaxel and surface-functionalized with poly(ethylene glycol) were used as model drug carriers. The results of the physicochemical characterization of the nanoparticles are summarized in Supplemental information (Table S1).

To study the diffusion of nanoparticles in fibrin matrices, we used a Transwell® assay. We found that the mobility of nanoparticles was significantly compromised by the matrix. No drug was detected in the receiver chamber through the time course of the experiment (Figure 2A). However, addition of tPA significantly improved the movement of nanoparticles. With an increase in the amount of tPA, the lag time (t_{lag}) for the appearance of drug in the receiver chamber decreased significantly (Figure 2B). To determine rate of drug transport from the top to bottom chamber we calculated Papp (Figure 2C). In the absence of tPA, there was no transport and Papp was zero. In the presence of 0.05 μg of tPA, Papp of the drug was 0.01 cm/h. With an increase in the amount of tPA to 0.5 μg, Papp nearly doubled. However further increase in tPA led to no change in Papp.

We also analyzed the cellular uptake of nanoparticles across fibrin gels. In these studies, nanoparticles were separated from a monolayer of B16F10 cells by fibrin matrix. As a positive control, we added nanoparticles directly to the cells. This resulted in a rapid uptake of nanoparticles. However, in the presence of the fibrin matrix, nanoparticle uptake was significantly reduced (Figure 2D). Addition of tPA resulted in a dose-dependent increase in cell uptake (Figure 2D–E). tPA had no effect on cellular uptake of nanoparticles in the absence of the fibrin gel (Figure S3).

These experiments show that fibrin matrix could significantly retard the movement of nanoparticles, and this effect could be reversed, at least partially, by co-treatment with tPA.

Safety and efficacy of combination therapy of paclitaxel nanoparticles and tPA

We determined the safety and tolerability of a combination of paclitaxel nanoparticles and tPA. Treatment with paclitaxel (as single therapy or in combination) led to a slight loss in body weight (~5%), which was recovered within 48 h of dosing (Figure S4 A–B). The levels of all the markers of liver function were elevated in response to paclitaxel therapy. Co-

administration of tPA did not have a significant impact on the body weight or the level of these markers (Figure S4 A–D)

We further evaluated the safety of tPA, and its effect on fibrin. Lung tumor bearing mice were treated with tPA, and blood D-dimer (a degradation product of fibrin) levels were analyzed using ELISA. In tumor bearing mice, treatment with tPA led to an increase in plasma levels of D-dimer protein. The increase in D-dimer levels was observed in tumor bearing mice but not in healthy mice (Figure S5). This suggests that tPA specifically degrades fibrin in tumor-bearing animals and does not have any detectable thrombolytic effect in healthy animals, providing further evidence to its safety.

We tested the efficacy of the combination of tPA and paclitaxel nanoparticles in a mouse orthotopic model of human lung cancer. Animals treated with paclitaxel in solution had a slower tumor growth rate as compared to saline treated animals. Paclitaxel in nanoparticles reduced the tumor growth rate even further. However, greatest tumor growth inhibition was seen when paclitaxel nanoparticles were administered in combination with tPA (Figure 3A).

We further tested the effect of tPA on the anticancer activity of paclitaxel in a syngeneic mouse melanoma model. Treatment with tPA or paclitaxel nanoparticles reduced tumor growth rate as compared to saline controls. Importantly, combining paclitaxel nanoparticles with tPA led to a further improvement in chemotherapeutic efficacy (Figure 3B). However, the improvement in efficacy with tPA co-administration was observed only at early time points in this more aggressive model.

Administration of tPA increases blood vessel diameter and tumor perfusion

Blood vessels in many solid tumors are compressed due to the presence of copious amounts of ECM components and a fast growing cell population. Previous experiments have shown that administration of cytotoxic therapies (6, 25) or ECM degrading enzymes (9) can decrease solid stress and restore vascular function. We hypothesized that degrading fibrin will have a similar effect.

Similar to that reported for other solid tumors (9), B16F10 tumors also had a significant number of collapsed blood vessels (Figures 4A and D). Most blood vessels were <10 μm in diameter. After treatment with paclitaxel nanoparticles, there was an increase in the median blood vessel diameter (Figure 4C and E). When treated with a combination of paclitaxel nanoparticles and tPA, the median vessel diameter increased even further (Figures 4B, C and F). It is interesting to note that regardless of the treatment, the diameter of most blood vessels was <10 μm. However, treatment with paclitaxel alone or in combination with tPA led to an increase in the number of blood vessels in the 10–20 μm diameter range (Figures 4D–F).

We further obtained real-time physiological information regarding blood perfusion in response to fibrinolytic therapy. Ultrasound imaging was used to track blood vessels in the subcutaneous B16F10 tumors. In saline treated animals, tumor perfusion area reached a maximum of ~1% after the second dose (Figure 4G and I). At all time points analyzed, tPA-treated tumors displayed a greater perfusion area (~3–4 fold higher) as compared to the

saline treated tumors. In animals treated with tPA, tumor perfusion area was maximal after the second dose (~4% of tumor area; $p<0.05$ vs saline-treated) (Figure 4H and I).

Co-administration of tPA increases penetration of Doxil® in the tumor core

We determined the effect of tPA administration on the intratumoral distribution of nanocarriers. Doxil® was used as a model anticancer nanomedicine in these studies because fluorescence of doxorubicin allows visualization of the drug in tissue sections.

In tumors treated with Doxil®, fluorescence intensity was higher towards the periphery and minimal in the interior regions of the tumor (Figure 5A). These results are in agreement with recent studies that show high drug accumulation in the tumor periphery as compared to that in the central core of the tumor (26). In tumors treated with a combination of tPA and Doxil®, fluorescence intensity was still maximal towards the periphery. However, compared to the control Doxil® group, greater distribution of doxorubicin-associated fluorescence intensity could be observed in the tumor interior (Figure 5B–C). These results indicate that treatment with tPA resulted in improved intratumoral distribution of Doxil®.

Interestingly, the distribution of Doxil® -associated fluorescence intensities in liver, lungs, spleen and brain cross sections were homogenous (Figure 5D–G, and Figure S6). This is in contrast to tumor sections which showed significantly lower fluorescence intensity in the core. Treatment with tPA did not affect the intra-tissue distribution of fluorescence. The total fluorescence intensity in tumors and other tissues were comparable between the Doxil and Doxil + tPA treated groups (Figure S7). This suggests that the overall biodistribution of Doxil is not affected by tPA co-therapy.

Discussion

Solid tumors are characterized by non-homogenous blood supply and the presence of varying degrees of hypoxia. These hypoxic regions often harbor aggressive and drug-resistant tumor cells (27). Thus, achieving therapeutic concentrations of the drug in these under-supplied regions of the tumor is a significant challenge.

Tumor blood vessels are formed in response to pro-angiogenic factors secreted by tumor cells (28). An imbalance in pro- and anti-angiogenic factors within the tumor tissue results in the formation of blood vessels that are abnormal and porous (29). Fluid leakage from these porous blood vessels and lack of functional lymphatics in the core of the tumor result in fluid accumulation in the tumor (30). This leads to diminished transvascular pressure gradient in certain regions of the tumor (30). Additionally, because of the presence of fast dividing cells within a limited volume and a highly dense ECM, blood vessels in the core of the tumor are compressed and not fully functional (7). Consequently, drug exchange through convection is highly compromised (5). Improving fluid dynamics in the tumor is, therefore, likely to have a significant impact on the delivery of drugs to tumors.

Several strategies have been used for improving drug transport within the tumor (31). The use of anti-angiogenics results in the normalization of blood vessels, leading to reduced fluid leakage out of the blood vessels, and a decrease in interstitial fluid pressure (29).

Consequently, convectional transport across blood vessels increases. On the other hand, decreasing the production or degrading the ECM in the tumor has also been shown to improve drug delivery. Decreasing the density of ECM can improve the diffusivity of the carrier/drug in the tumor matrix. Moreover, this can lead to decompression of the collapsed blood vessels, resulting in increased tumor perfusion and improved drug delivery (8, 9).

Due to the leaky nature of tumor blood vessels, there is significant fibrinogen deposition within the tumor. The prothrombogenic activity of the tumor microenvironment leads to the activation of fibrinogen to fibrin. The role of fibrin in tumor growth and metastasis has been well studied (32–35). During the initial stages of tumor growth, fibrin provides a scaffold for the growth of tumor cells. Fibrin also plays an important role in angiogenesis, modulating the influx of macrophages and in the storage of growth factors (36, 37). Depletion of fibrinogen may reduce formation of pulmonary metastatic foci. This effect is likely due to the loss of fibrinogen mediated protection of tumor cells against natural killer cells (34).

However, the role of fibrin in mediating solid stress and limiting drug delivery to tumors has not been studied extensively. In the current study, we used enzymatic degradation of fibrin to improve the delivery and chemotherapeutic efficacy of paclitaxel. Through immunohistochemistry studies, we found that treatment with tPA led to an increased blood vessel diameter. This data was supported by increased tumor perfusion as noted by ultrasound imaging. Importantly, co-administration of tPA led to an improved chemotherapeutic activity of paclitaxel nanoparticles in mouse models of melanoma and orthotopic lung cancer. A recent study analyzed the effect of tPA on the anticancer effect of nanoparticles in a xenograft subcutaneous A549 model (38). In agreement with our results, treatment with tPA led to an improved chemotherapeutic activity of nanoparticles. The benefit of co-treatment with tPA was different in the two tumor models used in our study. Thus, the type and location of the tumor may play a critical role in determining the improvement in activity obtained with tPA. Studying these effects in a transgenic tumor model or patient derived tumor models will likely provide additional mechanistic insights.

Previous studies have analyzed the expression of fibrin in animal tumor models (18, 19). However, a systematic analysis of fibrin expression in human tumors has not been performed previously. Fibrin levels in human tumor biopsies were variable, with no tumor type showing either a complete lack or consistently high level of fibrin. There are several reasons cited for this heterogeneity in fibrin expression. Current immunohistochemistry techniques cannot distinguish between fibrinogen and cross-linked fibrin. Additionally, bleeding during the collection of the tumor biopsy can also significantly affect the results (36). Accurately quantifying fibrin levels in tumors is important to successfully advance adjuvant fibrinolytic therapy. Novel peptides that specifically identify fibrin could be useful in this regard (39, 40).

We used a Transwell® assay to measure the mobility of nanoparticles through fibrin gels, and the influence of tPA on this mobility. Transwell® assays have been employed previously to characterize nanoparticle/drug transport across cell monolayers. In those assays, nanoparticle/drug transport commences upon their introduction into the top chamber. In contrast, in our experiment, due to the presence of a dense matrix of fibrin, drug was not

detected in the bottom chamber over the course of the study (10 h). Addition of tPA reduced the time to appearance of drug in the bottom chamber in a dose dependent manner. This indicates that fibrin gels used in our studies are resistant to nanoparticle transport. Additionally, transport across fibrin gels occurred in two phases. In the first phase characterized by digestion of fibrin gels by tPA, no drug deposition was seen in the bottom chamber. In the second phase, once the fibrin was digested, drug transport occurred at a constant rate. To quantify transport in both these phases, we used two parameters viz. lag time and apparent permeability. Lag time represents the time it takes for the gel to be digested, and apparent permeability represents the drug transport after fibrin digestion.

The clinical use of anti-coagulants and fibrinolytic therapies in cancer patients has been reported before (41–45). These studies have shown that administration of anti-coagulants such as heparin and warfarin improve mean survival in patients with small cell lung cancer. The rationale presented for the use of anti-coagulants is that it reduces the occurrence of spontaneous thromboembolism and tumor cell dissemination (44, 46). Some studies have reported the beneficial effects of using urokinase in conjunction with chemotherapy (41). The mechanism for the improved response to chemotherapy was not explored, however. In our studies, the benefit of tPA on the anti-cancer drug activity manifested itself through increased tumor vascularity, improved perfusion, and more uniform distribution of the drug within the tumor.

The use of tPA is contraindicated in patients with acute intracranial hemorrhage, severe uncontrolled hypertension, head trauma or stroke in previous three months, thrombocytopenia and coagulopathy, concomitant anti-coagulant therapy, severe hypoglycemia or hyperglycemia (47). Patients with these co-existing pathologies should be excluded from tPA co-therapy. Also, the presence of intracranial neoplasm is a contraindication for tPA therapy (48). However, tPA is not contraindicated for other cancers. Interestingly, there are several reports of patients with intracranial neoplasms who received IV thrombolysis but did not have intracranial hemorrhage (47, 49–51). Based on these reports, a recent review article (47) concluded that that intravenous thrombolysis can be safe in patients with intracranial neoplasms, provided the lesion is small and extra-axial in location. However, a careful assessment of benefit-to-risk ratio and co-morbidities is imperative before the clinical adoption of this strategy.

The time course of change in perfusion area with tumor volume is interesting. Perfusion area in untreated tumors and tPA treated tumors was highest after the second dose of tPA. Previous work has shown that blood flow generally decreases with an increase in tumor volume (52). The disparity in results may be due to different techniques used for measurement of blood flow. Lack of sensitivity of the ultrasound technique may have limited our ability to detect blood vessels in small tumors.

Studies with anti-angiogenic therapy have shown that there is a time window associated with the normalization of blood vessels (53, 54). In other words, the decrease in interstitial fluid pressure is transient. The improvement in drug delivery is maximal in this time window. It is conceivable that a similar phenomenon may occur with tPA treatment as well. Modeling reports suggest that an increased perfusion in leaky blood vessels can result in a rapid

increase in interstitial fluid pressure (55). This would quickly neutralize the advantage obtained with increased perfusion. Moreover, tPA has a short half-life. If the deposition of fibrin in tumors is rapid, the decrease in fibrin content of the tumor will likely be observed only for a short period of time. The pharmacokinetics of nanoparticles and tPA accumulation in the tumor may also be different. Additional studies are needed to determine the optimal frequency of tPA dosing and the time window following tPA dosing when the improvement in drug delivery is maximal. Further, we have only considered PLGA nanoparticles in this study. The effect of tPA co-delivery on other nanoparticulate systems of varying sizes would be of interest as well. A careful consideration of all these aspects can help maximize therapeutic benefits obtained from this strategy.

Conclusion

Poor vascular architecture and the consequent inadequate drug delivery limit the overall efficacy of chemotherapy. Fibrin deposition within the tumor can be an important cause for the compression of tumor blood vessels. Administration of tPA improved blood supply in solid tumors and enhanced chemotherapeutic activity of paclitaxel loaded polymeric nanoparticles.

Supplementary Material

Refer to Web version on PubMed Central for supplementary material.

Acknowledgments

Financial support: Funding was provided by the Center for Pharmaceutical Development, University of Minnesota (to J.P.) and the Doctoral Dissertation Fellowship, University of Minnesota (to A.R.K.).

We thank Drs. Sveotmir Markovic (Mayo Clinic) and Vladimir R. Muzykantov (University of Pennsylvania) for helpful discussions on the clinical use of fibrinolytics. The authors would like to thank Josh Parker (Comparative Pathology Shared Resource) for immunohistochemistry. Authors also acknowledge the Minnesota Supercomputing Institute for providing access to Matlab software. Live animal imaging (bioluminescence and ultrasound imaging) and confocal microscopy was performed at the University Imaging Center at the University of Minnesota. The authors also thank Mayank Verma and Dr. Guillermo Marques for providing training on ultrasound imaging and confocal microscopy.

References

1. Minchinton AI, Tannock IF. Drug penetration in solid tumours. Nat Rev Cancer. 2006; 6:583–92. [PubMed: 16862189]
2. Moghimi SM, Hunter AC, Murray JC. Long-circulating and target-specific nanoparticles: theory to practice. Pharmacol Rev. 2001; 53:283–318. [PubMed: 11356986]
3. Torchilin VP. Polymer-coated long-circulating microparticulate pharmaceuticals. J Microencapsul. 1998; 15:1–19. [PubMed: 9463803]
4. Albanese A, Tang PS, Chan WC. The effect of nanoparticle size, shape, and surface chemistry on biological systems. Annu Rev Biomed Eng. 2012; 14:1–16. [PubMed: 22524388]
5. Chauhan VP, Stylianopoulos T, Boucher Y, Jain RK. Delivery of molecular and nanoscale medicine to tumors: transport barriers and strategies. Annu Rev Chem Biomol Eng. 2011; 2:281–98. [PubMed: 22432620]
6. Padera TP, Stoll BR, Tooredman JB, Capen D, di Tomaso E, Jain RK. Pathology: cancer cells compress intratumour vessels. Nature. 2004; 427:695. [PubMed: 14973470]

7. Stylianopoulos T, Martin JD, Chauhan VP, et al. Causes, consequences, and remedies for growth-induced solid stress in murine and human tumors. Proc Natl Acad Sci U S A. 2012; 109:15101–8. [PubMed: 22932871]
8. Eikenes L, Bruland OS, Brekken C, de Davies CL. Collagenase increases the transcapillary pressure gradient and improves the uptake and distribution of monoclonal antibodies in human osteosarcoma xenografts. Cancer Res. 2004; 64:4768–73. [PubMed: 15256445]
9. Provenzano PP, Cuevas C, Chang AE, Goel VK, Von Hoff DD, Hingorani SR. Enzymatic targeting of the stroma ablates physical barriers to treatment of pancreatic ductal adenocarcinoma. Cancer Cell. 2012; 21:418–29. [PubMed: 22439937]
10. Brown LF, Van de Water L, Harvey VS, Dvorak HF. Fibrinogen influx and accumulation of cross-linked fibrin in healing wounds and in tumor stroma. Am J Pathol. 1988; 130:455–65. [PubMed: 3279791]
11. Brown LF, Dvorak AM, Dvorak HF. Leaky vessels, fibrin deposition, and fibrosis: a sequence of events common to solid tumors and to many other types of disease. Am Rev Respir Dis. 1989; 140:1104–7. [PubMed: 2478057]
12. Schafer M, Werner S. Cancer as an overhealing wound: an old hypothesis revisited. Nat Rev Mol Cell Biol. 2008; 9:628–38. [PubMed: 18628784]
13. Toti US, Guru BR, Grill AE, Panyam J. Interfacial activity assisted surface functionalization: a novel approach to incorporate maleimide functional groups and cRGD peptide on polymeric nanoparticles for targeted drug delivery. Mol Pharm. 2010; 7:1108–17. [PubMed: 20527782]
14. Roger E, Kalscheuer S, Kirtane A, et al. Folic acid functionalized nanoparticles for enhanced oral drug delivery. Mol Pharm. 2012; 9:2103–10. [PubMed: 22670575]
15. Patil Y, Sadhukha T, Ma L, Panyam J. Nanoparticle-mediated simultaneous and targeted delivery of paclitaxel and tariquidar overcomes tumor drug resistance. J Control Release. 2009; 136:21–9. [PubMed: 19331851]
16. Hubatsch I, Ragnarsson EG, Artursson P. Determination of drug permeability and prediction of drug absorption in Caco-2 monolayers. Nat Protoc. 2007; 2:2111–9. [PubMed: 17853866]
17. Sadhukha T, Wiedmann TS, Panyam J. Inhalable magnetic nanoparticles for targeted hyperthermia in lung cancer therapy. Biomaterials. 2013; 34:5163–71. [PubMed: 23591395]
18. Dvorak HF, Senger DR, Dvorak AM. Fibrin as a component of the tumor stroma: origins and biological significance. Cancer Metastasis Rev. 1983; 2:41–73. [PubMed: 6193869]
19. Brown LF, Asch B, Harvey VS, Buchinski B, Dvorak HF. Fibrinogen influx and accumulation of cross-linked fibrin in mouse carcinomas. Cancer Res. 1988; 48:1920–5. [PubMed: 3280123]
20. Eikenes L, Tari M, Tufto I, Bruland OS, de Lange Davies C. Hyaluronidase induces a transcapillary pressure gradient and improves the distribution and uptake of liposomal doxorubicin (Caelyx) in human osteosarcoma xenografts. Br J Cancer. 2005; 93:81–8. [PubMed: 15942637]
21. Eikenes L, Tufto I, Schnell EA, Bjorkoy A, De Lange Davies C. Effect of collagenase and hyaluronidase on free and anomalous diffusion in multicellular spheroids and xenografts. Anticancer Res. 2010; 30:359–68. [PubMed: 20332440]
22. Collen D. Fibrin-selective thrombolytic therapy for acute myocardial infarction. Circulation. 1996; 93:857–65. [PubMed: 8598075]
23. Zivin JA. Acute stroke therapy with tissue plasminogen activator (tPA) since it was approved by the U.S. Food and Drug Administration (FDA). Ann Neurol. 2009; 66:6–10. [PubMed: 19681102]
24. Goldhaber SZ. Contemporary pulmonary embolism thrombolysis. Chest. 1995; 107:45S–51S. [PubMed: 7813329]
25. Griffon-Etienne G, Boucher Y, Brekken C, Suit HD, Jain RK. Taxane-induced apoptosis decompresses blood vessels and lowers interstitial fluid pressure in solid tumors: clinical implications. Cancer Res. 1999; 59:3776–82. [PubMed: 10446995]
26. Ekdawi SN, Stewart JM, Dunne M, et al. Spatial and temporal mapping of heterogeneity in liposome uptake and microvascular distribution in an orthotopic tumor xenograft model. J Control Release. 2015; 207:101–11. [PubMed: 25862513]
27. Teicher BA. Hypoxia and drug resistance. Cancer Metastasis Rev. 1994; 13:139–68. [PubMed: 7923547]

28. Carmeliet P, Jain RK. Angiogenesis in cancer and other diseases. Nature. 2000; 407:249–57. [PubMed: 11001068]
29. Jain RK. Normalization of tumor vasculature: an emerging concept in antiangiogenic therapy. Science. 2005; 307:58–62. [PubMed: 15637262]
30. Heldin CH, Rubin K, Pietras K, Ostman A. High interstitial fluid pressure - an obstacle in cancer therapy. Nat Rev Cancer. 2004; 4:806–13. [PubMed: 15510161]
31. Kirtane AR, Kalscheuer SM, Panyam J. Exploiting nanotechnology to overcome tumor drug resistance: Challenges and opportunities. Adv Drug Deliv Rev. 2013; 65:1731–47. [PubMed: 24036273]
32. Costantini V, Zacharski LR. The role of fibrin in tumor metastasis. Cancer Metastasis Rev. 1992; 11:283–90. [PubMed: 1423819]
33. Palumbo JS, Potter JM, Kaplan LS, Talmage K, Jackson DG, Degen JL. Spontaneous hematogenous and lymphatic metastasis, but not primary tumor growth or angiogenesis, is diminished in fibrinogen-deficient mice. Cancer Res. 2002; 62:6966–72. [PubMed: 12460914]
34. Palumbo JS, Talmage KE, Massari JV, et al. Platelets and fibrin(ogen) increase metastatic potential by impeding natural killer cell-mediated elimination of tumor cells. Blood. 2005; 105:178–85. [PubMed: 15367435]
35. Palumbo JS, Kombrinck KW, Drew AF, et al. Fibrinogen is an important determinant of the metastatic potential of circulating tumor cells. Blood. 2000; 96:3302–9. [PubMed: 11071621]
36. Nagy JA, Brown LF, Senger DR, et al. Pathogenesis of tumor stroma generation: a critical role for leaky blood vessels and fibrin deposition. Biochim Biophys Acta. 1989; 948:305–26. [PubMed: 2465781]
37. Lu da Y, Chen XL, Ding J. Treatment of solid tumors and metastases by fibrinogen-targeted anticancer drug therapy. Med Hypotheses. 2007; 68:188–93. [PubMed: 16956730]
38. Zhang B, Jiang T, She X, et al. Fibrin degradation by rtPA enhances the delivery of nanotherapeutics to A549 tumors in nude mice. Biomaterials. 2016; 96:63–71. [PubMed: 27149664]
39. Starmans LW, van Mourik T, Rossin R, Verel I, Nicolay K, Grull H. Noninvasive visualization of tumoral fibrin deposition using a peptidic fibrin-binding single photon emission computed tomography tracer. Mol Pharm. 2015; 12:1921–8. [PubMed: 25922977]
40. Tsai YT, Zhou J, Weng H, Tang EN, Baker DW, Tang L. Optical imaging of fibrin deposition to elucidate participation of mast cells in foreign body responses. Biomaterials. 2014; 35:2089–96. [PubMed: 24342726]
41. Calvo FA, Hidalgo OF, Gonzalez F, et al. Urokinase combination chemotherapy in small cell lung cancer. A phase II study. Cancer. 1992; 70:2624–30. [PubMed: 1330286]
42. Elias EG, Brugarolas A. The role of heparin in the chemotherapy of solid tumors: preliminary clinical trial in carcinoma of the lung. Cancer Chemother Rep. 1972; 56:783–5. [PubMed: 4349928]
43. Elias EG, Shukla SK, Mink IB. Heparin and chemotherapy in the management of inoperable lung carcinoma. Cancer. 1975; 36:129–36. [PubMed: 1203841]
44. Zacharski LR, Henderson WG, Rickles FR, et al. Effect of warfarin on survival in small cell carcinoma of the lung. Veterans Administration Study No. 75. JAMA. 1981; 245:831–5. [PubMed: 6257941]
45. Altinbas M, Coskun HS, Er O, et al. A randomized clinical trial of combination chemotherapy with and without low-molecular-weight heparin in small cell lung cancer. J Thromb Haemost. 2004; 2:1266–71. [PubMed: 15304029]
46. Agnelli G, George DJ, Kakkar AK, et al. Semuloparin for thromboprophylaxis in patients receiving chemotherapy for cancer. N Engl J Med. 2012; 366:601–9. [PubMed: 22335737]
47. Fugate JE, Rabinstein AA. Absolute and Relative Contraindications to IV rt-PA for Acute Ischemic Stroke. Neurohospitalist. 2015; 5:110–21. [PubMed: 26288669]
48. Jauch EC, Saver JL, Adams HP Jr, et al. Guidelines for the early management of patients with acute ischemic stroke: a guideline for healthcare professionals from the American Heart Association/American Stroke Association. Stroke. 2013; 44:870–947. [PubMed: 23370205]

49. Rubinshtein R, Jaffe R, Flugelman MY, Karkabi B, Lewis BS. Thrombolysis in patients with a brain tumour. Heart. 2004; 90:1476. [PubMed: 15547033]
50. Han S, Chaya C, Hoo GW. Thrombolytic therapy for massive pulmonary embolism in a patient with a known intracranial tumor. J Intensive Care Med. 2006; 21:240–5. [PubMed: 16855059]
51. Mittal MK, Seet RC, Zhang Y, Brown RD Jr, Rabinstein AA. Safety of intravenous thrombolysis in acute ischemic stroke patients with saccular intracranial aneurysms. J Stroke Cerebrovasc Dis. 2013; 22:639–43. [PubMed: 22341666]
52. Kallinowski F, Schlenger KH, Runkel S, et al. Blood flow, metabolism, cellular microenvironment, and growth rate of human tumor xenografts. Cancer Res. 1989; 49:3759–64. [PubMed: 2736517]
53. Lin MI, Sessa WC. Antiangiogenic therapy: creating a unique “window” of opportunity. Cancer Cell. 2004; 6:529–31. [PubMed: 15607955]
54. Winkler F, Kozin SV, Tong RT, et al. Kinetics of vascular normalization by VEGFR2 blockade governs brain tumor response to radiation: role of oxygenation, angiopoietin-1, and matrix metalloproteinases. Cancer Cell. 2004; 6:553–63. [PubMed: 15607960]
55. Stylianopoulos T, Jain RK. Combining two strategies to improve perfusion and drug delivery in solid tumors. Proc Natl Acad Sci U S A. 2013; 110:18632–7. [PubMed: 24167277]

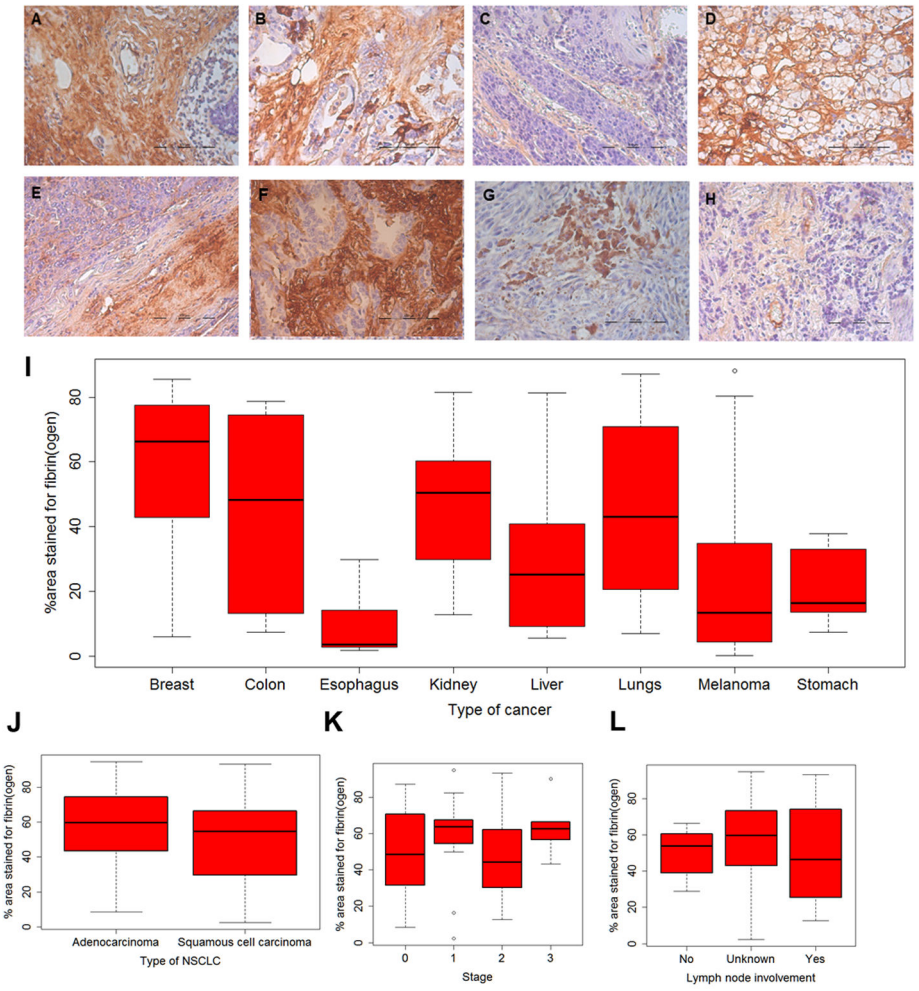

Figure 1. Fibrin(ogen) staining of human tumor biopsies

Tissue microarrays of human tumors were stained for fibrin(ogen). Shown here are representative images of fibrin(ogen) staining for cancers of (**A**) breast, (**B**) colon, (**C**) esophagus, (**D**) kidney, (**E**) liver, (**F**) lungs, (**G**) melanoma, and (**H**) stomach. Scale bar in (A)–(H) is 100 μm. (**I**) shows fraction of area stained for fibrin(ogen). For lung tumors, 228 images of samples acquired from 59 patients were analyzed. For melanoma, 120 images of samples acquired from 30 patients were analyzed. For the other tumor types, 20 images of samples acquired from 5 patients were analyzed. (**J–L**) show fibrin(ogen) staining in non-small cell lung carcinomas as a function of type, stage and lymph node involvement.

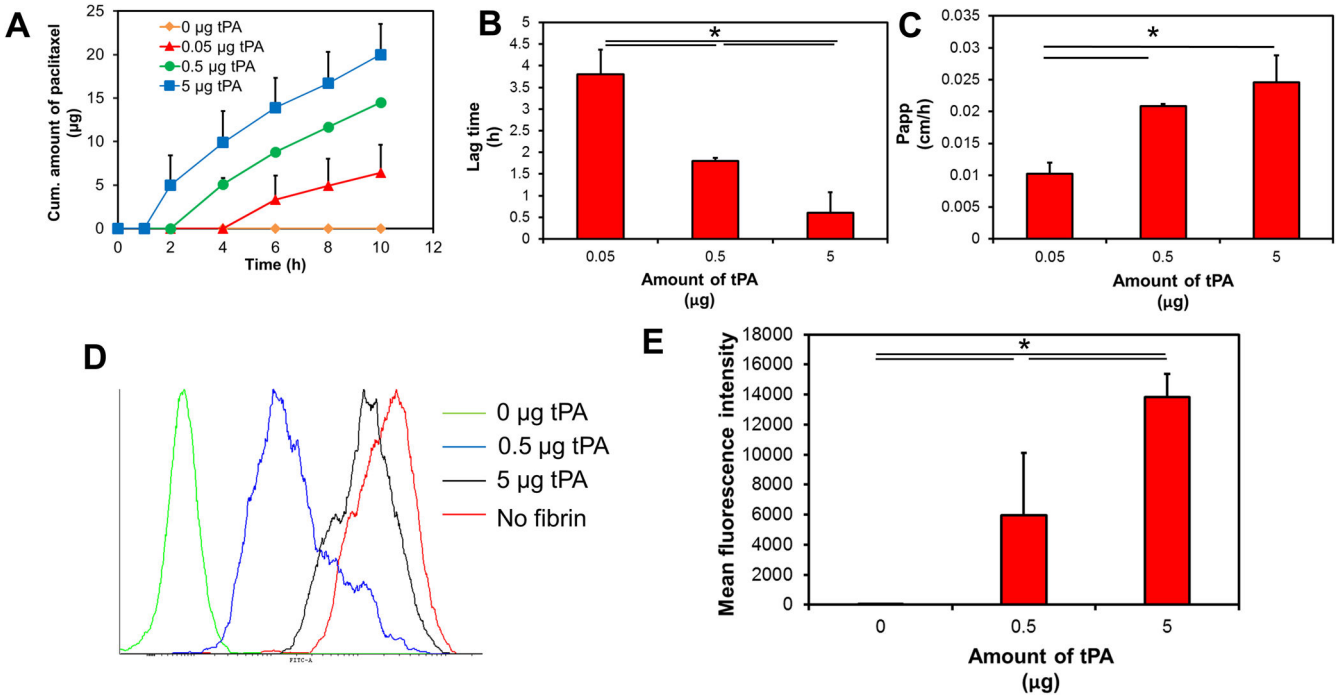

Figure 2. Effect of tPA on nanoparticle mobility in fibrin gels

Transwell® assay was used to analyze the migration of nanoparticles (with or without tPA) across fibrin matrix. (**A**) Cumulative amount of paclitaxel accumulating in the bottom chamber as a function of time. (**B**) Lag time for the first appearance of paclitaxel in the bottom chamber with increasing amounts of tPA. Results are represented as mean ± S.D., n=3, *p<0.05, one-way ANOVA. (**C**) Apparent permeability of paclitaxel from the top to bottom chamber. Data represented as mean ± S.D., n=3, *p<0.05, one-way ANOVA (**D**) Cellular uptake of nanoparticles across fibrin gels was determined using Transwell® assay. Representative histograms indicating cellular uptake of fluorescently labeled nanoparticles. (**E**) Quantitation of cellular uptake of nanoparticles as function of tPA concentration. Results are represented as mean ± S.D., n=4, *p<0.05, one-way ANOVA.

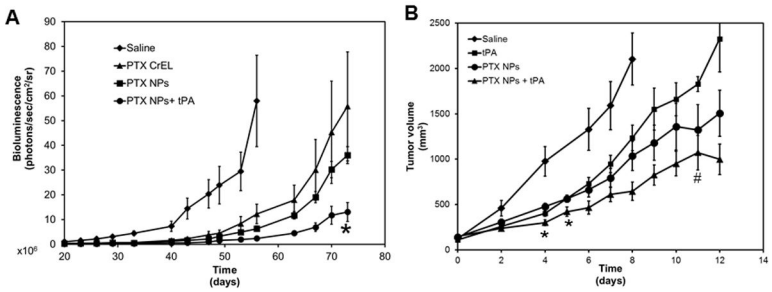

Figure 3. Efficacy of paclitaxel nanoparticles-tPA combination therapy

(**A**) SCID-beige mice bearing orthotopic lung tumors were treated with paclitaxel. Tumor growth was monitored by measuring bioluminescence using IVIS *in vivo* imaging. Results shown as mean ± S.E.M, n=5–6, *p<0.05 compared to paclitaxel nanoparticles, Student's t-test (**B**) C57Bl/6 mice bearing subcutaneous B16F10 melanoma tumors were treated with tPA, or paclitaxel nanoparticles or a combination of paclitaxel nanoparticles and tPA. Tumor volumes were measured over time using a digital caliper. Data represented as mean ± S.E.M., n=6–9 animals/group. *p<0.05 compared to paclitaxel nanoparticles, # indicates p<0.05 compared to tPA, Student's t-test

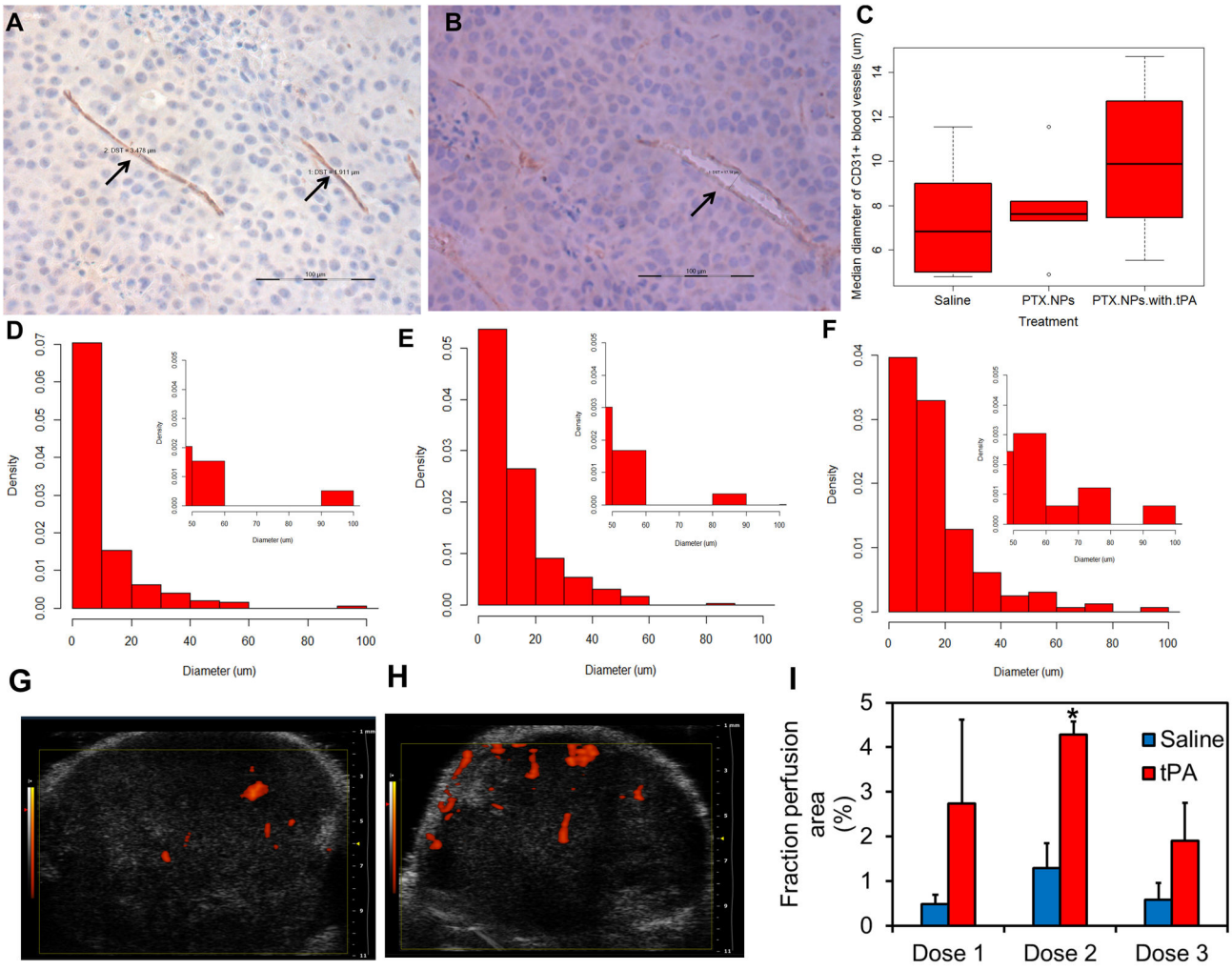

Figure 4. Effect of tPA treatment on tumor blood vessel diameter and tumor perfusion

Representative pictures showing (**A**) compressed blood vessel (arrows) in saline-treated tumor and (**B**) decompressed blood vessel (arrow) in a tumor treated with tPA-paclitaxel nanoparticle combination therapy. Scale bar in A and B is 100 μm. (**C**) Median tumor blood vessel diameter in animals that received different treatments. Representative histograms showing tumor blood vessel diameter in animals treated with (**D**) saline, (**E**) paclitaxel nanoparticles, and (**F**) paclitaxel nanoparticles and tPA. B16F10 tumor bearing animals were treated with three doses of saline or tPA. Ultrasound images were taken after each dose. Representative sonograms of B16F10 tumors after receiving the second dose of (**G**) saline or (**H**) tPA. (**I**) Mean perfusion area in saline or tPA treated tumors. Data represented as mean ± S.E.M., n=3–5, *p<0.05, Student's t-test.

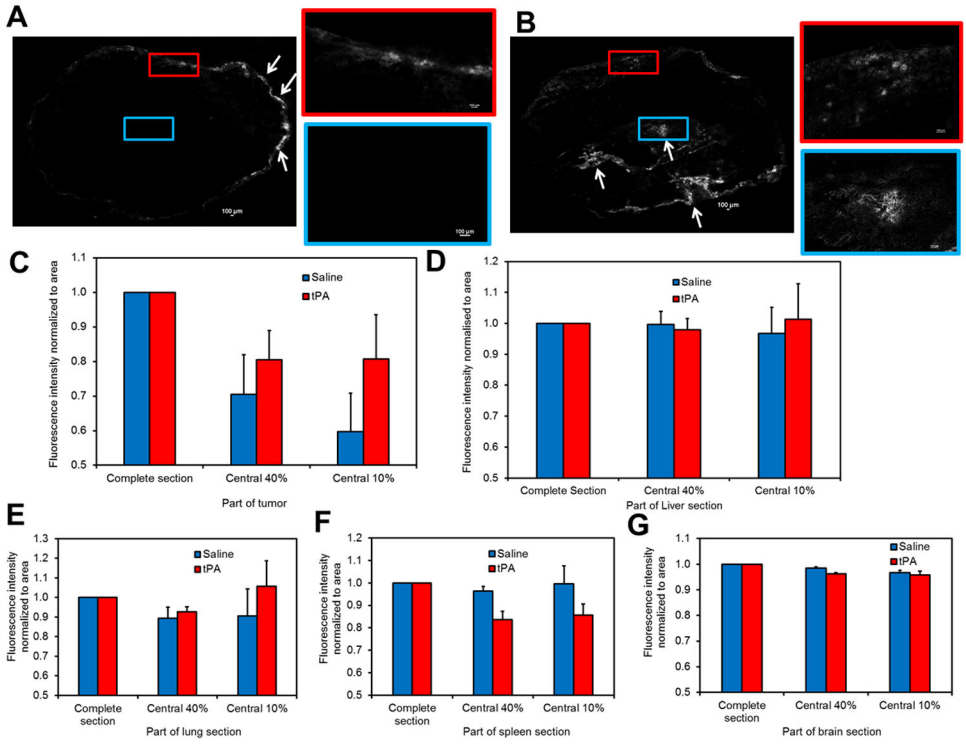

Figure 5. Intratumoral and intraorgan distribution of Doxil® in B16F10 tumors

Tumor bearing mice were treated with either Doxil or a combination of Doxil and tPA. Animals were sacrificed 24 h later, tumors were collected and fluorescence of doxorubicin was imaged using confocal microscopy. Shown here are representative micrographs of tumors treated with (**A**) Doxil® or (**B**) combination of Doxil® and tPA. Arrows indicate fluorescence in tumor sections. Relative fluorescence intensity normalized to area in the entire tissue section and the central 40% and 10% of the tissue area in (**C**) tumor (**D**) liver (**E**) lung (**F**) spleen (**G**) brain. Data is represented as mean ± S.E.M., n=3 animals/group. Three tumor sections and one section of normal tissue from each animal were analyzed.